Flow rate-independent electrical aerosol sensor

A. Rostedt* and J. Keskinen

Aerosol Physics, Laboratory of Physics, Tampere University of Technology, Tampere, Finland

*corresponding author, e-mail: antti.rostedt@tut.fi

Flow rate-independent electrical aerosol sensor

Abstract

A new diffusion charging–based aerosol instrument design is presented, intended to be a starting point for a low-cost particle concentration sensor. The aim in the design is to minimize instrument response dependence on the sample flow rate. The operation principle, response functions of the components, and performance of a prototype instrument are reported. Based on the performance evaluation, the instrument response remained constant within ±15% over a wide sample flow rate range of 3 to 10 lpm. While in the design some sensitivity is sacrificed to minimize flow rate dependency, the detection limit is still sufficient for a practical sensor application.

Introduction

Increased awareness of the adverse health effects of air pollutants has led to a growing need for up-to-date air quality information. This information is usually expressed as an Air Quality Index, which combines the measurement results of different pollutants such as nitrogen dioxide (NO_2), ozone (O_3), and particulate matter (PM). Apart from the official air quality measurement sites, there is growing interest in simplified instruments that provide supporting information on air quality (Snyder et al., 2013). Such instruments could be deployed in sensor networks having wide coverage over urban areas. As a result, more localized information could be obtained, which could then be used to follow the dispersion of pollutants from their emission sources and to support localized air quality forecasts. Following this approach, Gao et al. (2015) demonstrated a network of 8 optical sensors for monitoring urban area particle concentrations.

The recent development of low-cost optical particle sensors has made it possible to construct affordable instruments based on optical particle detection. Holstius et al. (2014) presented an extensive study on one such instrument in field conditions. Although dependent on particle density and refractive index, the output of these devices can be calibrated to measure the mass concentration of practical ambient aerosols with reasonable accuracy. However, while perfectly feasible for coarse mode particle concentration monitoring, these instruments miss the ultrafine particles (UFPs). Furthermore, instead of the mass concentration, the health effects of UFPs are often related to other metrics such as the lung deposited surface area (LDSA) of the particles (Brown et al., 2001). Conveniently, the output of the electrical aerosol instruments based on diffusion charging is sensitive to UFPs and correlates well with the LDSA (Wilson et al., 2007). These facts have led to the development of instruments such as those presented by Fissan et al. (2007), Marra et al. (2010), Fierz et al. (2011), and Fierz et al. (2014) that target UFP concentration monitoring.

The simplest approach to electrical aerosol measurement consists of a diffusion charger, an ion collecting trap, a particle collecting filter inside a Faraday cage, an electrometer to measure the electric current, and a pump to provide the sample flow. While forming a working setup for particle measurement, it does, however, have two drawbacks when considering the sensor application. First is the particle filter, which forms a considerable pressure drop in the flow system that increases with the collected particles. The second drawback is that the output is, in the first approximation, proportional to the product of particle

concentration and sample flow rate. Because of this, the operation of these instruments requires continuous information on the flow rate. In practice the sample flow is usually kept constant by an active control. Neither of these shortcomings is insurmountable, but they may become relevant when minimizing the cost of a particle sensor. The particle collecting filter can be omitted by using non-collecting particle charge measurement techniques, such as presented by Lehtimäki (1983) and Fierz et al. (2014). A diffusion charging–based instrument operating in changing flow conditions was presented in Rostedt et al. (2009b), but the processing of the measured data required external information on the flow rate.

In this article we present an approach for a low-cost electrical aerosol instrument design, for which the response is relatively independent of the sample flow rate. Additionally, as the instrument does not require a filter for particle collection, the pressure drop in the flow system can be minimized. Both of these features promote the use of a low-cost fan or an external means for supplying the sample flow. For instance, low-cost axial fans can be used for generating the sample flow. Such fans are capable of producing a maximum pressure difference only in the order of 100 Pa, which makes the flow rate susceptible to small pressure changes, such as those caused by the dynamic pressure of the wind.

Operating principle and instrument response

The instrument design is based on a unipolar diffusion charger combined with charge detection via electrical particle collection. The particles are first charged, and then some of the charged particles are collected from the sample flow by an electrostatic particle collector. One of the key features of the design is that only a fraction of the particles are collected. The output of the instrument is the measured current carried by the collected particles. A schematic view of the sensor construction is shown in figure 1. The charger and the electrostatic collector components used in the prototype have not been optimized for sensor-type operation. However, they enable proof of concept measurements on achievable instrument performance.

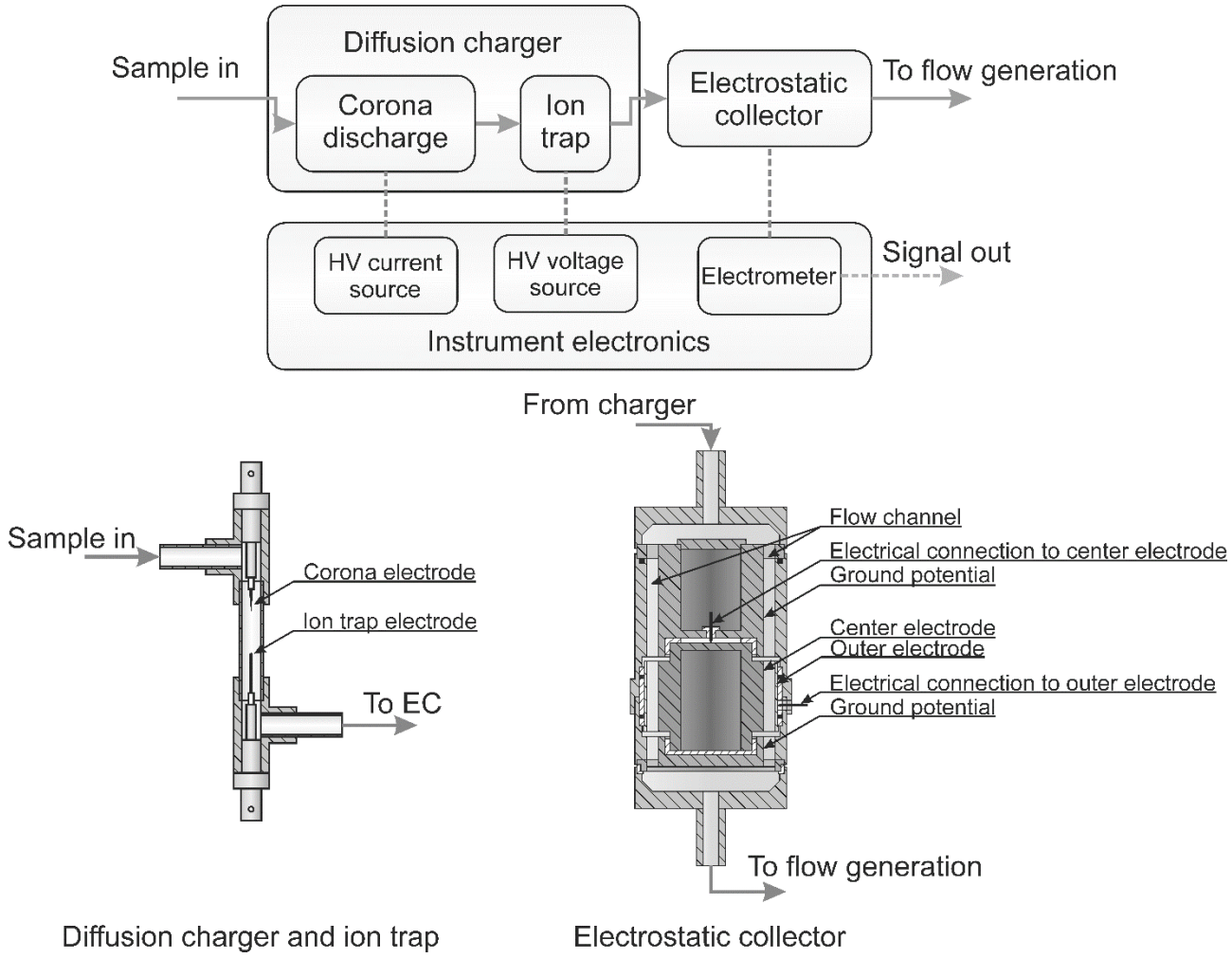

Figure 1. Schematic view of the instrument design together with cross-section views of the components. The cross-section view of the mobility analyzer used here as the electrostatic particle collector is adapted from Rostedt et al. (2009a).

Particle size dependent response. Adding a term for the fraction of current collected by the electrostatic collector, the electrical current measured by the diffusion charging–based instrument can be written following Dhaniyala et al. (2011):

$$I(d_p) = R_i\left(d_p\right)N\left(d_p\right) = E_{ch}\left(d_p\right)r_{ec}N\left(d_p\right)$$
$$R_i\left(d_p\right) = E_{ch}\left(d_p\right)r_{ec} \quad (1)$$

The instrument response $R_i(d_p)$ gives the measured current for a given particle number concentration $N(d_p)$ in units of Am^3 or, as below, $fAcm^3$. The particle size dependent instrument response is the product of the charger response E_{ch} ($fAcm^3$) and the current fraction measured from the electrostatic collector r_{ec} (dimensionless). The charger response (E_{ch}) is written as

$$E_{ch}\left(d_p\right) = P_{ch}\left(d_p\right)n_{ave}\left(d_p\right)eQ_s, \quad (2)$$

where e is the elementary charge and Q_s is the volumetric flow rate. The $P_{ch}n_{ave}$ product (e.g., Marjamäki et al., 2000) is the product of particle penetration through the charger P_{ch} and the number of elementary charges per particle n_{ave}, both dependent on the particle diameter. After the charger, particles of a certain diameter have a distribution of elementary charges, often approximated as log-normal (e.g., Kaminski et al., 2012). The charge number n_{ave} above is the arithmetic mean value of the number of elementary charges per particle, which is in practice calculated by dividing the number of elementary charges by the number of all particles. It follows from this definition that both P_{ch} and n_{ave} take into account all particles, including those remaining neutral. As discussed by Virtanen et al. (2001), taking into account only the charged particles would change the values of P_{ch} and n_{ave} but would lead to the same value for the product. For most of the particle diameter values discussed below, the fraction of neutral particles is negligible and therefore both definitions produce the same value for P_{ch} and n_{ave}.

The measured current signal comes from the particles collected by an electrostatic field in the electrostatic collector. The current fraction measured from an electrostatic collector is linked to the collection efficiency η_{ec}. For a particle with an electrical mobility of Z, the collection efficiency is simply

$$\eta_{ec} = \frac{Z}{Z_0} = \frac{neB}{Z_0}, \tag{3}$$

where ne is the charge of the particle and B is the mechanical mobility of the particle: $B = C_C / 3\pi\eta_g d_p$. The characteristic electrical mobility Z_0 of the collector depends on the collector geometry and voltage. For the annular geometry used in the prototype, the term Z_0 can be written in the form of equation 4 (see, e.g., Fuchs, 1964).

$$Z_0 = Q_s \frac{\ln(s_o/s_i)}{2\pi V_{ec} l_e} \tag{4}$$

The terms in equation 4 are the volumetric flow rate Q_s, the inner and outer diameters of the annular slit (s_i and s_o), the collection voltage V_{ec}, and the length of the collection electrode l_e. Equation (3) is only valid for $Z \leq Z_0$; the collection efficiency is one for particles with a higher electrical mobility.

The fraction of the total current measured from the electrostatic collector would equal the collection efficiency if the particles were equally charged. For the charge distribution exiting the charger, the current fraction r_{ec} (dimensionless) can be written as

$$r_{ec}\left(d_p\right) = \frac{n_{qm}\left(d_p\right) eB\left(d_p\right)}{Z_0} \tag{5}$$

This equation is valid only if the collection efficiency for all existing particle diameter and charge combinations is below 1. The number of charges per particle is here substituted by an effective number of charges per particle n_{qm}. It is a characteristic of the charge distribution but different from the average value n_{ave} related to equation 2. As discussed in more detail in the supplementary information, the effective number of charges takes the form of

$$n_{qm} = \frac{\sum_{n=0}^{\infty} c_n n^2}{\sum_{n=0}^{\infty} c_n n} \tag{6}$$

Equation 6 is a function of particle diameter, although not explicitly shown. The averaging is for a single particle diameter, over the charge distribution. In the notation, c_n is the fraction of particles carrying n elementary charges. Note that n_{qm} is not affected by the neutral particles. The value of this quantity can also be experimentally obtained, as described later. It should be stressed that for the operation window of the present approach, particle charge and the characteristic electrical mobility Z_0 need to be controlled so that r_{ec} is less than unity for all the particles.

The flow dependence of the instrument response will be treated next. As discussed above, the instrument response function is the product of the charger response and the current fraction of the collected particles. Combining equations 1, 2, and 5, the response takes the form of equation 7:

$$\begin{aligned} R_i &= P_{ch}(Q_S) n_{ave}(Q_S) e Q_s \frac{2\pi n_{qm}(Q_S) eB}{Q_s} \frac{V_{ec} l_e}{\ln(s_o/s_i)} \\ &= K P_{ch}(Q_S) n_{ave}(Q_S) n_{qm}(Q_S) B \end{aligned} \tag{7}$$

Equation 7 is written as a function of the sample flow rate, omitting particle size dependence. In the last form, all the constant factors have been multiplied to one constant marked with K. An interesting outcome of equation 7 is that as long as the collection efficiency of the electrostatic collector is below 1 for all particles, the direct effect of sample flow rate is cancelled out from the instrument response. The product $P_{ch}n_{ave}n_{qm}$ is still in principle dependent on the flow rate. The charged particle losses in the charger decrease with decreasing residence time in the electric field. Therefore, the particle penetration through the charger P_{ch} increases with increasing flow rate Q_s. The number of elementary charges per particle (n_{ave}) and the effective charge number n_{qm} are related through the charge distribution. The value of $n_{ave}n_{qm}$ product depends on the product of the residence time and ion concentration in the charger ($N_i t$ product; Davison et al., 1985). The $N_i t$ product is approximately inversely proportional to the flow rate, while the dependence of n_{ave} and n_{qm} on $N_i t$ is logarithmic. Therefore, there should be a region where the increase in penetration and decrease in charge numbers with increasing flow rate minimize the flow rate dependency of the instrument response.

Methods

To test the proposed instrument design, a prototype instrument was constructed consisting of a diode-type corona discharge diffusion charger, combined with an annular electrostatic particle collector. Cross sections of the instrument components are shown in figure 1. Inside the charger, a sharpened tungsten rod acted as the discharge electrode, and it was placed inside a cylindrical flow channel with diameter of 8 mm. During the experiments, the charger was operated with a constant 20 µA current, with a discharge voltage of approximately 4.2 kV. After the charger, the ions were removed from the flow with an ion trap. The trap geometry was annular with an 8 mm outer diameter, 1.2 mm inner diameter, and the voltage electrode length was approximately 15 mm. The voltage electrode was set to 400 V potential, which was sufficient for removing all the ions at least up to 20 lpm flow rate. For particle detection, the add-on mobility analyzer

designed for the Electrical Low Pressure Impactor (ELPI; Rostedt et al., 2009a) was used as the electrostatic particle collector. The inner and outer diameters of the electrostatic collector were 45 mm and 55 mm, respectively, and the effective length of the particle collection electrode was 33 mm. The collection voltage was set to 80 V. After the electrostatic collector, the remaining ELPI impactor stages were replaced with a spacer tube, leaving only the ELPI filter stage. The current measured from the filter was used only for the charger characterization measurements. The measured current signals were recorded with the ELPI electrometers.

The constructed prototype instrument was characterized with laboratory test measurements. Both the charger operation with different sample flow rates, and the instrument response were studied. The measurement setups used in the characterization measurements are shown in figure 2. The test aerosol generation and size distribution monitoring setup is shown on the left panel of figure 2. The test aerosol was generated using a singly charged aerosol reference (SCAR; Yli-Ojanperä et al., 2010). The advantage of the SCAR is that all the generated particles contain only one elementary charge, and after subsequent classification with a differential mobility analyzer (DMA; TSI, Inc., model 3071), monodisperse test aerosol was obtained, with particle diameters ranging from 25 to 500 nm. The DMA was operated in a closed-loop setup (Jokinen and Mäkelä, 1997) with the flow circulating unit (FCU) and without the aerosol neutralizer. In order to have sufficient concentration for the measurement, the DMA sample to sheath air ratio was set to 1:5, which widened slightly the size distribution of the classified particles. In order to cover a wide particle size range, two sheath air flow rate values, 10 and 5 lpm, were used with the corresponding sample flow rate values of 2 and 1 lpm, respectively. The generated monodisperse particles were all singly charged, but prior to passing to the instrument the aerosol was brought to bipolar charge equilibrium using a ^{241}Am ionization source. The bipolar equilibrium state was preferred over absolutely neutral particles, as the former is expected to be closer to the measured aerosol state in real applications. After passing through the neutralizer, the aerosol was diluted by a dilution air feed to provide sufficient sample flow for the prototype instrument, and to ensure proper sample mixing, a flow mixer was placed after the dilution. The sample flow through the prototype instrument was controlled and measured with a mass flow controller (MFC, Alicat Scientific, Inc. MC-50SLPM-D/5M).

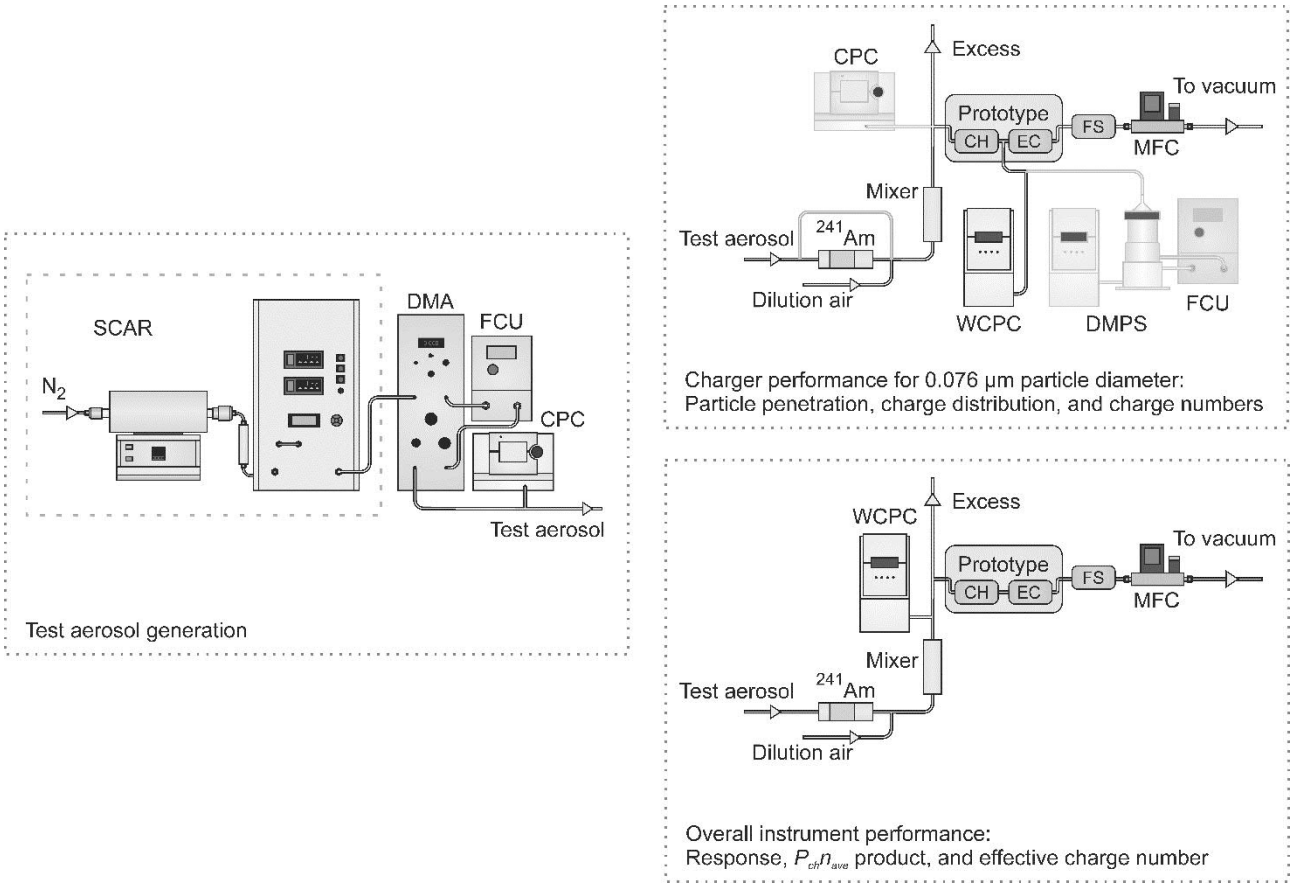

Figure 2. The laboratory test measurement setups used in the characterization measurements.

Charger (CH) performance was studied using the measurement setup shown in the top right panel of figure 2. Monodisperse aerosol sample flow was directed to the prototype instrument, and a small sample flow of 0.6 lpm was extracted to a water condensation particle counter (WCPC; TSI, Inc., model 3786) from between the charger and the electrostatic collector (EC). The ELPI filter stage (FS) was placed after the electrostatic collector in order to measure the total current after the charger. With this setup, the average charge number (n_{ave}) was obtained by comparing the total current, measured as the sum of the electrostatic collector and the filter stage currents, to the number concentration measured by the WCPC, taking into account the differences in the flow rates. The effective charge number was obtained by dividing the current measured from the electrostatic collector with the total current and then solving equation 5 for n_{qm}. The particle penetration through the charger was studied by comparing the number concentration measured by the WCPC with the charger switched on and off. As the measurements were not simultaneous, the data were corrected for the minor variations of the test aerosol concentration that were monitored with a condensation particle counter (CPC TSI, Inc., model 3776). With this setup, the charge numbers and the particle penetration were studied at 0.076 µm particle diameter in the flow rate range from 2 to 20 lpm. Using this same setup, it was also possible to measure the particle charge distribution after the charger by replacing the WCPC with a differential mobility particle sizer (DMPS). The DMPS consisted of a model 3085 DMA (TSI, Inc.) and the 3786 WCPC. During the measurements, the ^{241}Am neutralizer was briefly bypassed to verify the operation of the electrostatic particle collector with singly charged particles.

The measurement setup shown in the lower right panel of figure 2 was used for characterizing the instrument's performance with monodisperse test aerosol. The key performance parameters obtained were the $P_{ch}n_{ave}$ product value, the effective charge number of the particles n_{qm}, and the instrument response R_i. The charger response was obtained by dividing the total current (i.e. the sum of currents measured from the electrostatic collector and the filter) by the total number concentration measured with the WCPC. From this, the $P_{ch}n_{ave}$ product value was calculated by dividing the charger response by the elementary charge and the sample flow rate. From the measured data, the value for the effective charge number (n_{qm}) was obtained in the same manner as above. The instrument response R_i was obtained by dividing the current measured from the electrostatic particle collector by the total number concentration measured by the WCPC.

The prototype instrument was also tested with polydisperse test aerosol with different sample flow rates in the range of 4.5–10 lpm using the measurement setup shown in figure 3. An evaporation condensation generator (Liu and Lee, 1975) was used as the test aerosol generator, with dioctyl sebacate (DOS) as the particle material. After the generator, the aerosol was diluted with an ejector dilutor (ED1) to lower the concentration and to provide sufficient flow for the instruments. The particle size distribution was measured using a scanning mobility particle spectrometer (SMPS), consisting of a model 3071 DMA (TSI, Inc.) operated with a closed loop and a model 3776 CPC (TSI, Inc.). A WCPC model 3786 (TSI, Inc.) was used to measure the total number concentration to improve the concentration measurement accuracy. An additional ejector dilutor (ED2) was used in front of the WCPC to lower the concentration to the WCPC measurement range. The dilution ratio of the ED2 was 7.4, as measured separately after the tests. During the measurements, the test aerosol size distribution median size (d_m) varied between 0.033 and 0.170 µm, while the geometric standard deviation (GSD) varied between 1.31 and 1.52. More detailed information on the size distributions can be found in the supplementary information. The sample flow rate of the prototype instrument was controlled in the same manner as in the monodisperse characterization measurements.

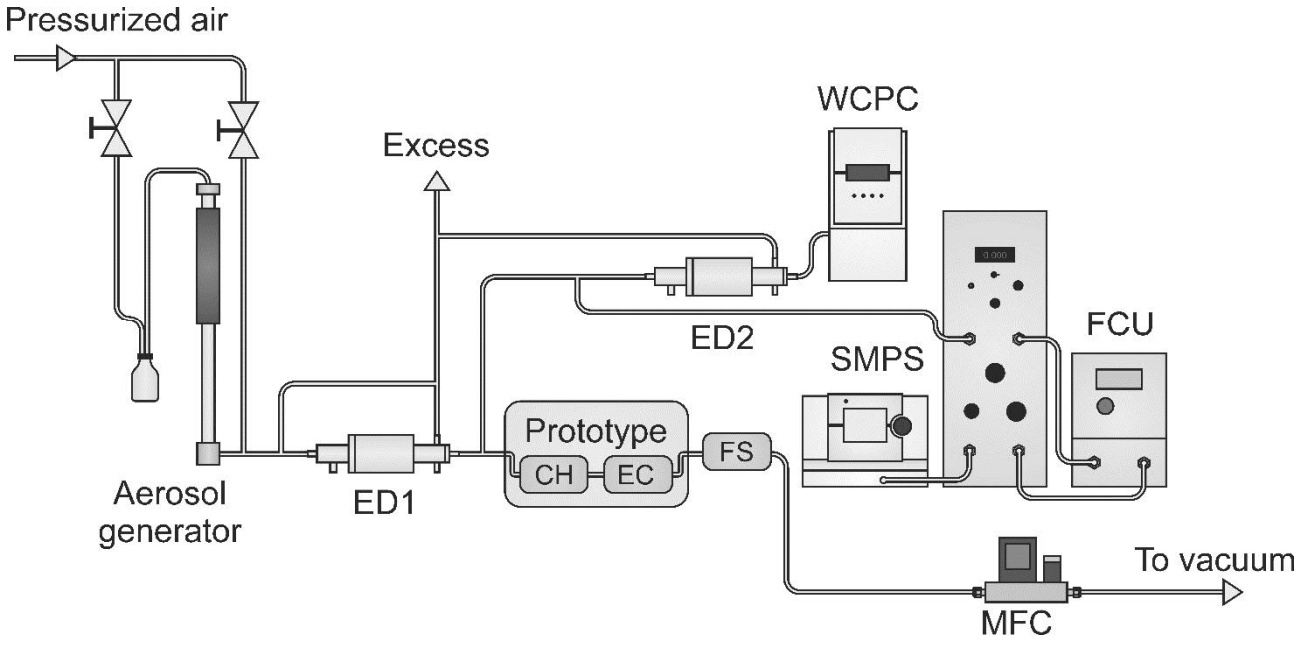

Figure 3. The measurement setup used in the polydisperse test measurements.

Response characterization

The effective number of charges per particle and charger operation. The particle charge distribution was measured using the measurement setup shown in the top right panel of figure 2. The distribution for 0.076 µm particles with a sample flow rate of 8 lpm is shown in figure 4. Because of the somewhat widened particle diameter range of the DMA classified test particles (see above), discrete values could only be resolved for the lowest charge numbers. Therefore, the mobility range was oversampled with the second DMA, and the distribution in figure 3 was treated as continuous. From the charge distribution, values for the average charge n_{ave} = 5.76 and for the effective number of charges per particle n_{qm} = 6.32 were calculated. These values are plotted as vertical lines in figure 3, together with the effective charge number value n_{qm} = 6.36 obtained simultaneously from the electrostatic collector current fraction. As expected, the effective number of charges is higher than the average value. The n_{qm} value obtained from the collected current fraction is slightly higher than that calculated from the charge distribution but is still considered to be a very good match.

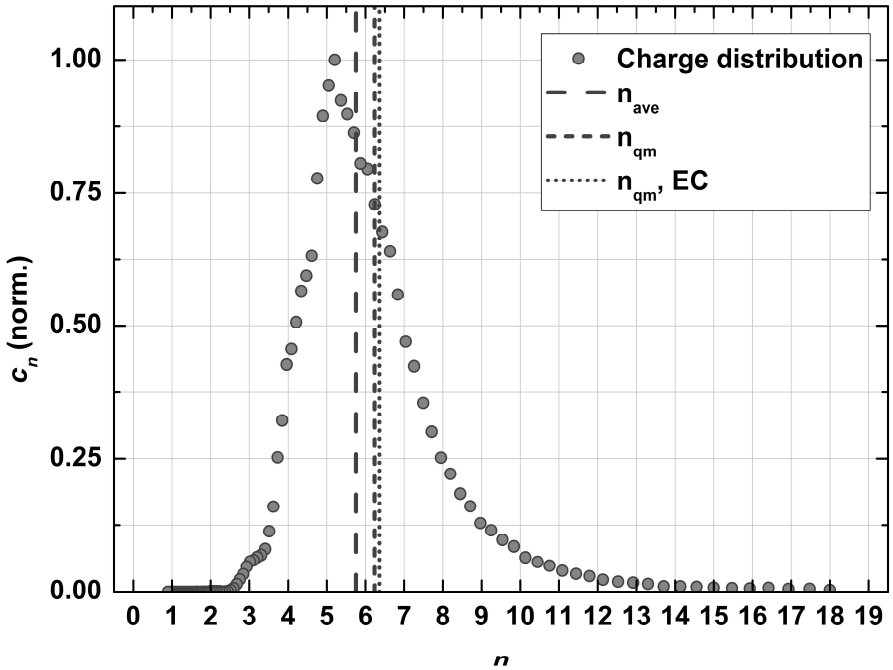

Figure 4. Particle charge distribution after the diffusion charger measured for 0.076 µm particles at 8 lpm sample flow rate. The average and effective charge numbers n_{ave} and n_{qm}, calculated from the charge distribution, are plotted as vertical lines. A corresponding value for the effective charge number obtained from the electrostatic collector current fraction is shown for comparison (n_{qm}, EC).

The average and effective charge numbers together with the particle penetration through the charger, measured for 0.076 µm diameter particles, are shown as functions of the sample flow rate in figure 5. As expected, the charge numbers decrease with increasing sample flow rate as a consequence of the decreasing $N_i t$ product, whereas the particle penetration through the charger increases. The particle penetration levels are close to unity for sample flow rates exceeding 10 lpm. The instrument response would decrease monotonically beyond this flow rate. The n_{ave} values experimentally obtained above do not take into account

the neutral particles, but the P_{ch} values do. However, the fraction of neutral particles is expected to be negligible here, meaning that their product is a valid $P_{ch}n_{ave}$ product also.

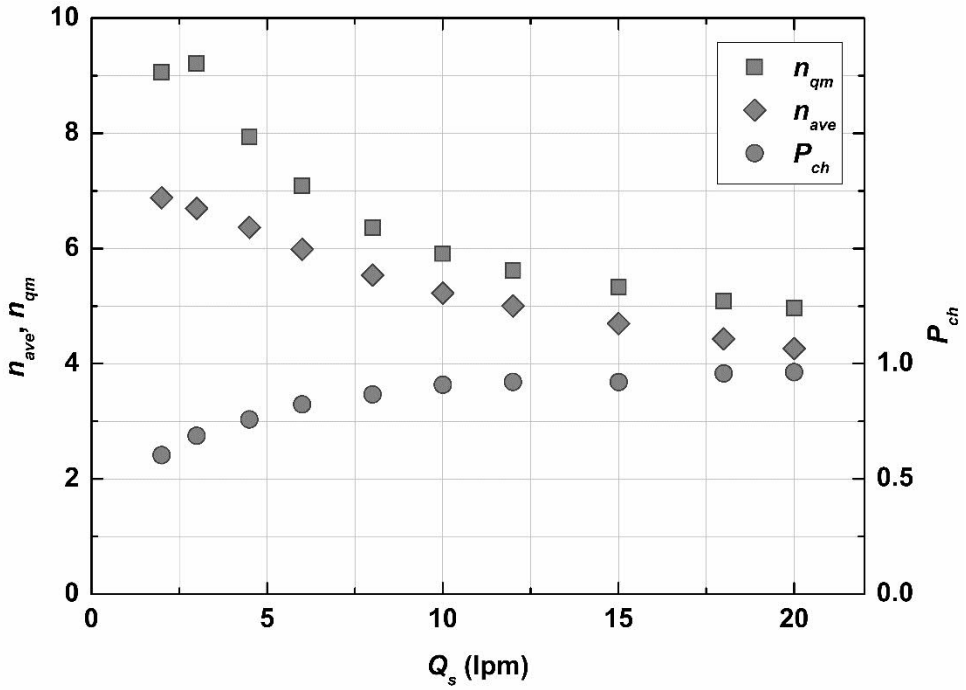

Figure 5. The effect of the sample flow rate on the charger operation measured for 0.076 µm particles: The average and effective charge numbers shown as the function of the sample flow rate.

Particle size dependent response. The $P_{ch}n_{ave}$ product value, as a function of particle diameter, was measured with the setup presented in the lower right panel of figure 2. This direct measurement of the $P_{ch}n_{ave}$ product is valid even if the number of particles remaining neutral is not negligible. The results obtained for sample flow rates 3, 4.5, 6, 8, and 10 lpm are shown in figure 6a together with a power function fit of equation 8. For fitting purposes, we define a dimensionless particle diameter $d_n = d_p / 1\ \mu m$.

$$P_{ch}n_{ave}\left(d_n\right) = 176\ d_n^{1.41} \tag{8}$$

The $P_{ch}n_{ave}$ product values for the lowest flow rate deviate from the rest, especially for particle diameters below 0.040 µm. These sample points are indicated by an arrow. This is interpreted to be caused by increased electrostatic losses in the electric field of the corona discharge zone of the charger. For the instrument response, the current fraction measured from the electrostatic particle collector (r_{ec}) for the charged particles is also required. This was obtained from the measured data by dividing the current measured from the electrostatic collector by the total current for each particle size. The measured current fractions are discussed in more detail in the supplementary information. The effective number of charges were calculated from the measured current fractions, and a power function was fitted to the data (equation 9). The obtained effective charge numbers together with the fit are plotted in figure 6b.

$$n_{qm}\left(d_n\right) = 224\ d_n^{1.37} \tag{9}$$

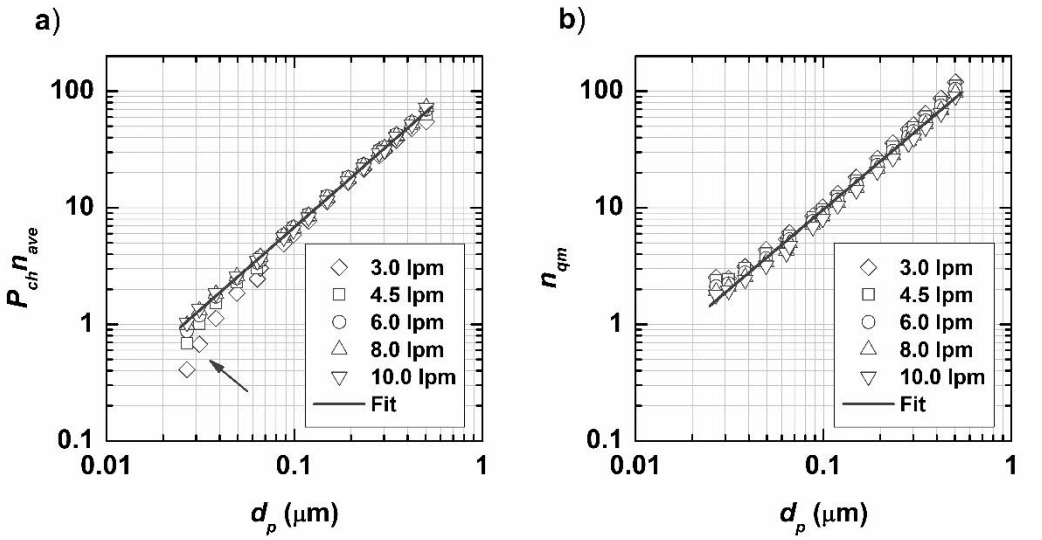

Figure 6. Particle diameter dependent values characterizing the charger, measured using different flow rates: a) $P_{ch}n_{ave}$ product as a function of particle diameter, together with the power function fit of equation 7. b) Effective charge (n_{qm}) as a function of particle diameter, together with the fit of equation 8.

The response of the prototype instrument was obtained by dividing the current measured from the electrostatic collector by the total number concentration measured with the reference WCPC. The results are plotted in figure 7 against particle diameter for different flow rates. The flow rate–independent form of the instrument response of equation 7 is shown in equation 10. Based on the instrument design parameters, the constant K takes the value of $K = 2.13 \cdot 10^{-36}$ Am^3kg/s in SI units.

$$R_i\left(d_p\right) = KP_{ch}n_{ave}\left(d_p\right)n_{qm}\left(d_p\right)B\left(d_p\right) \tag{10}$$

Using the dimensionless particle diameter d_n, and the fit values of equations 8 and 9, scaling the product of the constant values for more convenient current and concentration units, and introducing dimensionless particle mobility $B_n = B / B_0$, $B = 1$ s/kg, the response can be written as

$$R_i\left(d_n\right) = 8.38 \cdot 10^{-11} B_n\left(d_n\right) d_n^{2.78} \text{ fAcm}^3 \tag{11}$$

This instrument response fit is plotted with a solid line in figure 7 for comparison with the measured data points. The shaded area in the plot shows ±15% deviation from the fit. The measured instrument response remains quite well within 15% of the fitted response. The most significant deviation can be seen at the smallest particle diameter with the lowest flow rate value. This is due to the particle losses inside the charger, as discussed above. A power-law fit of d_p^1 for the diameter dependence describes the response reasonably well from 25 nm to 250 nm (figure S2). The obtained power value is lower than the power of the charger response due to the electrostatic particle collector's contribution to the instrument response.

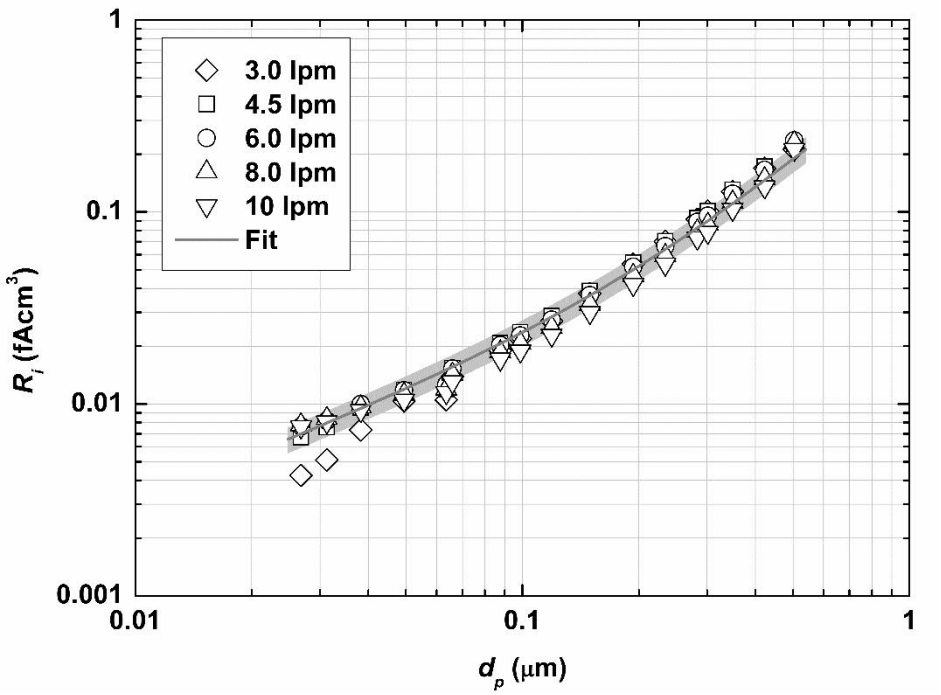

Figure 7. Measured response of the prototype instrument R_i, shown together with the response fit of equation 10.

The effect of the sample flow rate on the instrument response is plotted in figure 8, where the normalized responses for selected particle sizes are plotted as the function of the sample flow rate. The responses measured for different particle sizes are normalized to 0.97 at 8 lpm sample flow rate. The normalized responses remain within ±15% except again for lowest particle diameter with the lowest flow rate. These deviating points are beyond the operational range of the prototype.

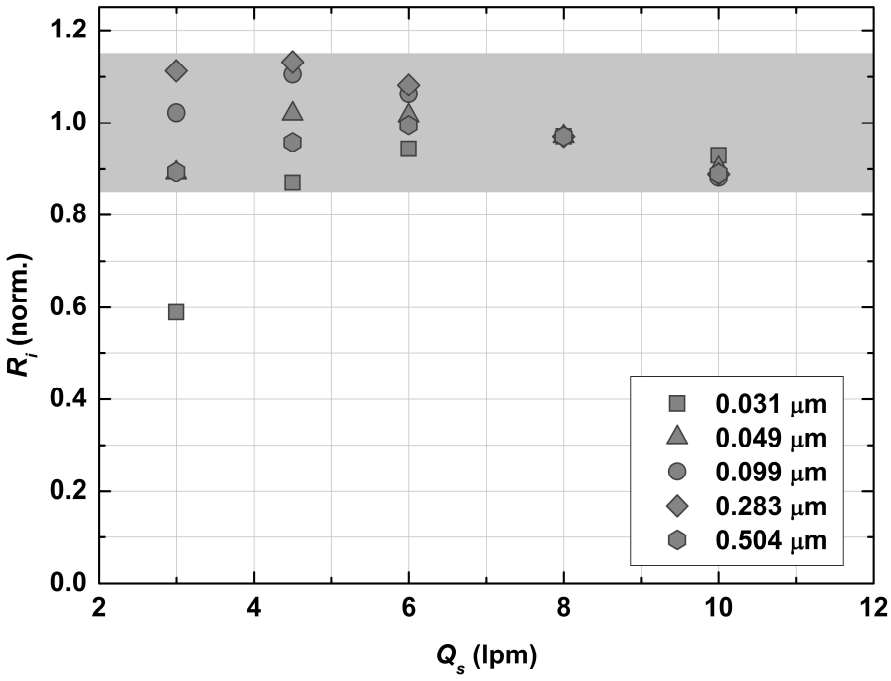

Figure 8. Normalized instrument responses as the function of the sample flow rate measured for four different particle sizes. The shaded area represents ±15% deviation from the average.

Polydisperse test measurements

The measured sensor output was compared to the simulated output signal based on the response fit. The starting point of the simulated output was the measured SMPS number size distribution ($N(d_p)$), which was normalized to the total number concentration measured by the WCPC. For each measured size distribution, the simulated (I_s) output was calculated according to equation 10.

$$I_s = \int R_s\left(d_p\right) N\left(d_p\right) dd_p \tag{10}$$

A correlation plot between the measured and simulated instrument outputs is shown in figure 9a. The points in the correlation plot measured with different flow rates overlap, indicating that the measurement result is virtually independent of the sample flow rate.

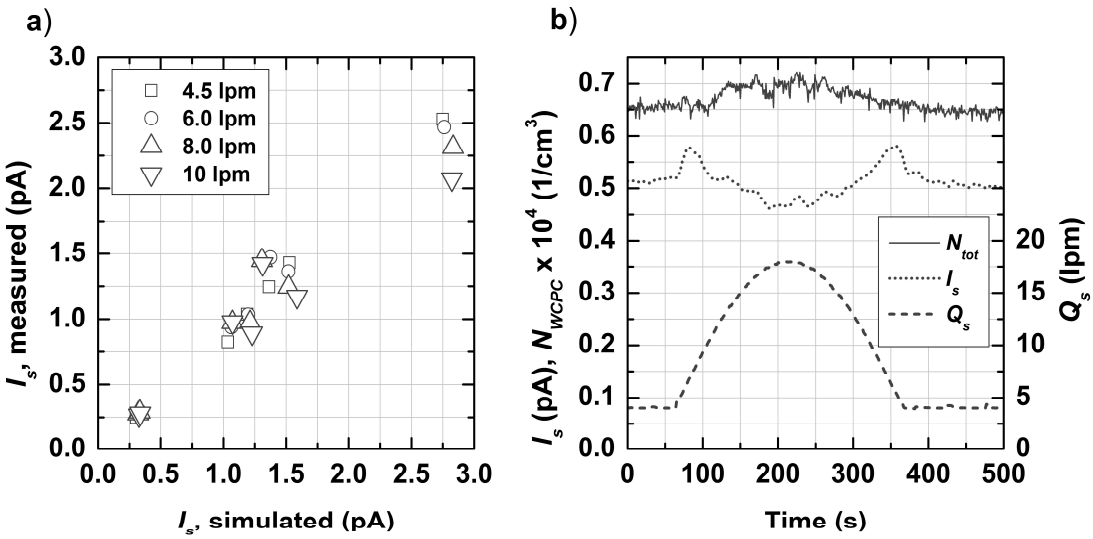

Figure 9. Polydisperse test measurement results: a) Correlation plot of the simulated and measured sensor outputs measured for the polydisperse test aerosol. b) Measured sensor output, total number concentration, and the sample flow rate during a flow rate ramp from 4.5 to 18 lpm and back to 4.5 lpm.

The flow rate independence of the measured instrument response is further demonstrated in figure 9b, showing a time plot of the instrument output when the flow rate is varied continuously over a rather wide range. The sample flow rate of the instrument and the measured total number concentration are plotted for reference. During the test the instrument flow rate was varied from 4.5 lpm to 18 lpm and back, while the aerosol generation was kept constant. The median size of the test aerosol was 0.042 µm and the GSD of the size distribution 1.41. There is a small variation in the instrument output, but the maximum variation in the signal is approximately ±12%. The variation in the input total number concentration was approximately ±7% during the experiment.

Summary and discussion

A design approach for a low-cost electrical aerosol instrument was presented. The aim in the design was to minimize the instrument output sample flow rate dependence. The performance of a prototype instrument was demonstrated in laboratory measurements, where the instrument response and the effect of the sample flow rate were studied, resulting in a fit for the response.

The instrument was characterized for the flow rate range of 3 to 10 lpm. Within this flow range, the variation caused by the flow rate in the instrument response was approximately ±15% for particle sizes ranging from 0.040 to 0.500 µm. For particles below 0.040 µm, the variation increases for low flow rates because of decreased particle penetration through the charger. To keep the response variation within 15%, the minimum flow rate of the current prototype is limited to 4.5 lpm if a significant fraction of the current signal originates from particles below 0.040 µm. For this, the count median size of the size distribution needs to be below 0.040 µm. The upper limit of 10 lpm is caused by a response decrease with decreasing particle charge number. Both of these limitations originate from the charger design. Criteria looser or stricter than the 15% adapted here would obviously lead to wider or narrower acceptable flow rate ranges, respectively.

Within the presented concept, the operational flow rate range of an instrument can be tailored by changing the charger and electrostatic particle collector dimensioning. The designed maximum flow rate could range from a few liters to hundreds of liters per minute. Because of the open construction, the pressure drop in the instrument can be minimized. This would allow for the use of a low-cost fan to supply the sample flow but also for applications where the flow is produced independently of the instrument.

Electrical aerosol instruments are often used to measure the aerosol condensation sink (Kuuluvainen et al., 2010) or the LDSA concentration (Wilson et al., 2007). For the latter, the instrument response is often tailored by electrical particle collection as first introduced by Fissan et al. (2007). In the presented instrument design approach, tailoring the particle size dependence of the instrument is not as straightforward as for fixed flow rate designs. For ultrafine particles the obtained size dependence of the instrument response ($\sim d_p^1$) is somewhat lower than what is used in the diffusion charging–based instruments targeted for the measurement of the LDSA concentration (Todea et al., 2015). The performance of this type of instrument in measuring the condensation sink or the LDSA will, however, be a subject of further study.

In the design, some instrument sensitivity is sacrificed to minimize the effect of the varying sample flow rate on the response. Despite this, the sensitivity is still adequate for a practical application. For a very conservative detection limit of 10 fA for the electrical current, the detection limit in concentration would be approximately 400 1/cm^3 for an aerosol size distribution having a count median diameter of 0.10 µm and a geometric standard deviation of 1.5. This is comparable to the sensitivity of other non-collecting diffusion charging–based instruments such as presented by Fierz et al. (2014) and Rostedt et al. (2014). The instrument design requires a high-stability voltage source as the variations of the particle collection voltage are capacitively coupled to the electrometer current signal. However, as the required power level is extremely low, effective filtering can be applied in the voltage source.

References

Brown, D., Wilson, M., MacNee, W., Stone, V., Donaldson, K., 2001. Size-dependent proinflammatory effects of ultrafine polystyrene particles: a role for surface area and oxidative stress in the enhanced activity of ultrafines. Toxicol. Appl. Pharmacol. 175 (3), 191-199.

Davison, S. W., Hwang, S. Y., Wang, J., and Gentry, J. W. (1985) Unipolar Charging of Ultrafine Particles by Diffusion of Ions: Theory and Experiment. Langmuir 1985:1, 150-158.

Dhaniyala, S.; Fierz, M.; Keskinen, J. Marjamäki, M. (2011) Instruments based on electrical detection of aerosols. in: Aerosol Measurement: Principles, Techniques, and Applications, 3rd Edition, (ed. Kulkarni, Pramod; Baron, Paul A.; Willeke, Klaus) John Wiley & Sons, 393-413.

Fierz, M., Houle, C., Steigmeier, P., and Burtscher, H. (2011). Design, Calibration, and Field Performance of a Miniature Diffusion Size Classifier. Aerosol Sci. Technol., 45(1):1–10.

Fierz, M., Meier, D., Steigmeier, P., and Burtscher, H. (2014). Aerosol Measurement by Induced Currents. Aerosol Sci. Technol., 48:350–357.

Fissan, H., Neumann, S., Trampe, A., Pui, D., and Shin, W. (2007). Rationale and Principle of an Instrument Measuring Lung Deposited Nanoparticle Surface Area. J. Nanopart. Res., 9:53–59.

Fuchs, N. A. (1964)). The mechanics of aerosols. Oxford: Pergamon Press.

Gao, M., Cao, J., and Seto, E. (2015). A distributed network of low-cost continuous reading sensors to measure spatiotemporal variations of PM2.5 in Xi'an, China. Environmental Pollution 199:56-65

Holstius, D. M., Pillarisetti, A., Smith, K. R., and Seto, E. (2014). Field calibrations of a low-cost aerosol sensor at a regulatory monitoring site in California. Atmos. Meas. Tech. Discuss., 7, 605–632.

Jokinen, V. and Mäkelä, J. M. (1997) Closed-loop arrangement with critical orifice for DMA sheath/excess flow system. J. Aerosol Sci. 28, 4:643-648.

Kaminski, H., Kuhlbusch, T., Fissan, H., Ravi, L., Horn, H.-G., Han, H.-S., Caldow, R., and Asbach, C. (2012). Mathematical Description of Experimentally Determined Charge Distributions of a Unipolar Diffusion Charger. Aerosol Sci. Technol., 46:708–716.

Kuuluvainen, H., Kannosto, J., Virtanen, A., Mäkelä, J. M., Kulmala, M., Aalto, P., and Keskinen, J. (2010). Technical Note: Measuring condensation sink and ion sink of atmospheric aerosols with the electrical low pressure impactor (ELPI). Atmos. Chem. Phys., 10, 1361–1368

Lehtimäki, M. (1983). In Modified Electrical Aerosol Detector. in Aerosols in the Mining and Industrial Work Environments, Vol. 3, V. A. Marple, and B. Y. H. Liu, eds., Ann Arbor Science Publishers, Ann Arbor, pp. 1135–1143.

Liu, B.Y.H. and Lee, K.W. (1975). An Aerosol Generator High Stability. Am. Ind. Hyg. Assoc. J. 36: 861-865.

Marjamäki, M., Keskinen, J., Chen, D-R., and Pui, D. Y. H. (2000). Performance Evaluation of Electrical Low Pressure Impactor (ELPI). J. Aerosol Sci., 31:249–261.

Marra, J., Voetz, M. and Kiesling, H.-J. (2010). Monitor for detecting and assessing exposure to airborne nanoparticles. J. Nanopart. Res. 12:21–37.

Rostedt, A., Arffman, A., Janka, K., Yli-Ojanperä, J. and Keskinen, J., (2014) Characterization and Response Model of the PPS-M Aerosol Sensor. Aerosol Sci. Technol., 48:10, 1022-1030.

Rostedt, A., Marjamäki, M., and Keskinen, J., (2009a). Modification of the ELPI to Measure Mean Particle Effective Density in Real-Time. J. Aerosol Sci., 40:823–831.

Rostedt, A., Marjamäki, M., Yli-Ojanperä, J., Keskinen, J., Janka, K., Niemelä,V. and Ukkonen, A., (2009b) Non-Collecting Electrical Sensor for Particle Concentration Measurement. AAQR, 9:470–477, doi: 10.4209/aaqr.2009.03.0023

Snyder, E. G., Watkins, T. H., Solomon, P.A, Thoma, E. D., Williams, R. W., Hagler, G. S. W., Shelow, D., Hindin, D. A., Kilaru, V. J. and Preuss P. W., (2013) The Changing Paradigm of Air Pollution Monitoring. Environ. Sci. Technol. 47, 11369–11377, doi: 10.1021/es4022602

Tammet, H. F., 1970. The aspiration method for the determination of atmospheric-ion spectra, Israel Program of Scientific Translations, Jerusalem, 1970.

Todea, A. M., Beckmann, S., Kaminski, H. and Asbach, C. (2015) Accuracy of electrical aerosol sensors measuring lung deposited surface area concentrations. J. Aerosol Sci., 89:96-109.

Virtanen, A., Marjamäki, M., Ristimäki, J. and Keskinen, J. (2001) Secondary particle collection mechanisms in ELPI. J. Aerosol Sci., 32:389–401.

Wilson, W., Stanek, J., Han, H.-S., Johnson, T., Sakurai, H., Pui, D., Turner, J., Chen, D.-R., Duthie, S. (2007). Use of the electrical aerosol detector as an indicator of the surface area of fine particles deposited in the lung. J. Air Waste Manag. Assoc. 57(2), 211-220.

Yli-Ojanperä, J., Mäkelä, J. M., Marjamäki, M., Rostedt, A., and Keskinen, J. (2010). Towards Traceable Particle Number Concentration Standard: Single Charged Aerosol Reference (SCAR). J. Aerosol Sci., 41:719–728.

Supplementary information

Because the particle charge contributes to both the collection efficiency and the measured current, the fraction of total current measured from the electrostatic particle collector differs from the particle collection efficiency when the charge on the particles is distributed. Considering particles having the same mechanical mobility, the total measured current I_{tot} is the sum of the different charge fractions as shown in equation S1, where n is the number of elementary charges in the particle, c_n is the fraction of particles having n elementary charges, e is the elementary charge, and Q_s is the volumetric sample flow rate. N' is the particle number concentration at the inlet of the electrostatic particle collector. Here $N' = P_{ch}N$, where P_{ch} is the particle penetration through charger and N the number concentration at the inlet of the charger.

$$I_{tot} = \sum_{n=0}^{\infty} c_n N' neQ_s \tag{S1}$$

The current measured from the collected particles I_{ec} is the sum of the different charge fractions collected according to equation S2. The new terms in the equation are the particle mechanical mobility B and characteristic electrical mobility of the electrostatic collector Z_0.

$$I_{ec} = \sum_{n=0}^{\infty} c_n N' \frac{neB}{Z_0} neQ_s \tag{S2}$$

Now, for the fraction of the total current measured from the electrostatic collector, $r_{ec} = I_{ec} / I_{tot}$ can be written in the form of equation S3.

$$r_{ec} = \frac{\sum_{n=0}^{\infty} c_n n^2 eB}{\sum_{n=0}^{\infty} c_n n\, Z_0} = n_{qm} \frac{eB}{Z_0} \tag{S3}$$

Equation S3 has the same form as the particle collection efficiency (eq. 3), but the number of elementary charges is substituted by a weighted average charge n_{qm} of equation S4.

$$n_{qm} = \frac{\sum_{n=0}^{\infty} c_n n^2}{\sum_{n=0}^{\infty} c_n n} \tag{S4}$$

Note that taking into account only the charged particles (n > 0) would not change the value of n_{qm}.

The current fractions measured from the collected particles were measured in the laboratory characterization measurements. The results obtained for flow rates of 3, 6, and 10 lpm are presented in figure S1. Figure S1a shows the measured current fractions as a function of the particle size for different flow rates. Multiplying the measured fractions with the volumetric sample flow rate, as plotted in figure S1b, normalizes the direct effect of the flow rate. The remaining differences with different flow rates are caused by the decrease in effective particle charge with increasing flow rate. As seen in figure S1a, the collected current fraction is significantly below 1 for most of the measured data points, but reaches 1 at smallest particles for 3 lpm sample flow rate. Therefore, these points are beyond the operational range of the prototype instrument.

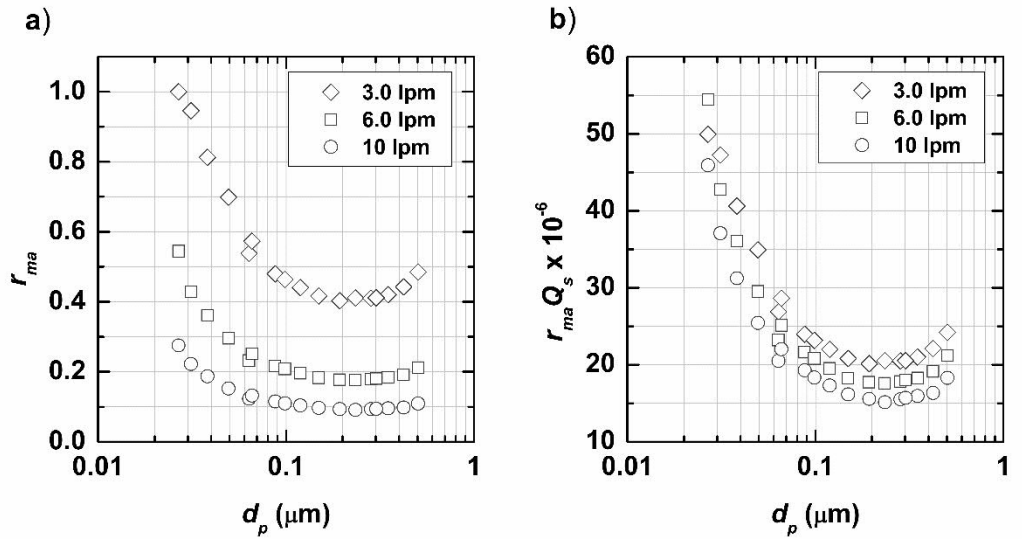

Figure S1. a) The collected current fractions measured from the electrostatic particle collector as a function of the particle size. b) The collected current fractions multiplied by the volumetric sample flow rate as a function of the particle size.

Figure S2 shows the measured overall instrument response function values with a power-law fit for the diameter dependence. The fitted power-law function gives a reasonable fit in the particle size range from 0.025 to 0.250 μm but underestimates the response for larger particles.

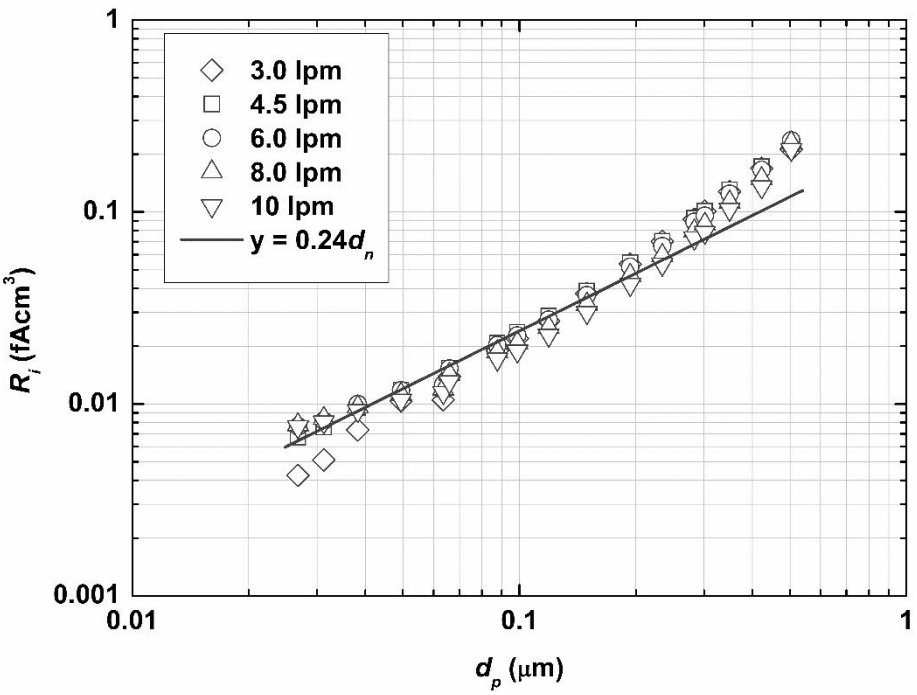

Figure S2. Measured response of the prototype instrument R_i, shown together with a d_p^1 power-law fit for the diameter dependence the response.

The statistical data of the test aerosol size distributions used in the polydisperse test measurements are collected in table S1. The measured size distributions are plotted in figure S3.

Table S1. Statistical data on the lognormal size distribution used in the polydisperse test measurements. Count median size (d_m), geometric standard deviation (GSD), and total number concentration (N_{tot}) shown.

Distribution	d_m (μm)	GSD	N_{tot} (1/cm³)
1	0.033	1.31	1.59×10^5
2	0.039	1.35	1.04×10^5
3	0.043	1.44	2.45×10^4
4	0.052	1.44	5.60×10^4
5	0.084	1.48	8.43×10^4
6	0.130	1.48	3.56×10^4
7	0.167	1.52	2.96×10^4

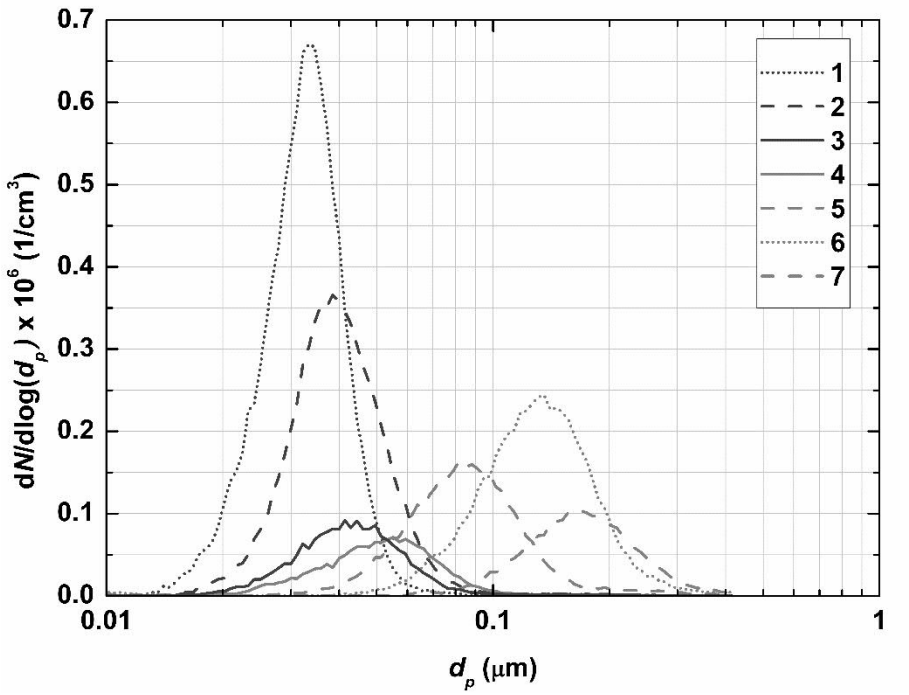

Figure S3. Measured size distributions in the polydisperse test measurements.